Lawrence Berkeley Laboratory
UNIVERSITY OF CALIFORNIA

Materials & Molecular
Research Division

Submitted to the Journal of Nuclear Materials

INTERPRETATION OF TRACER SURFACE DIFFUSION EXPERIMENTS ON UO_2 ROLES OF GAS AND SOLID TRANSPORT PROCESSES

D.R. Olander

June 1980

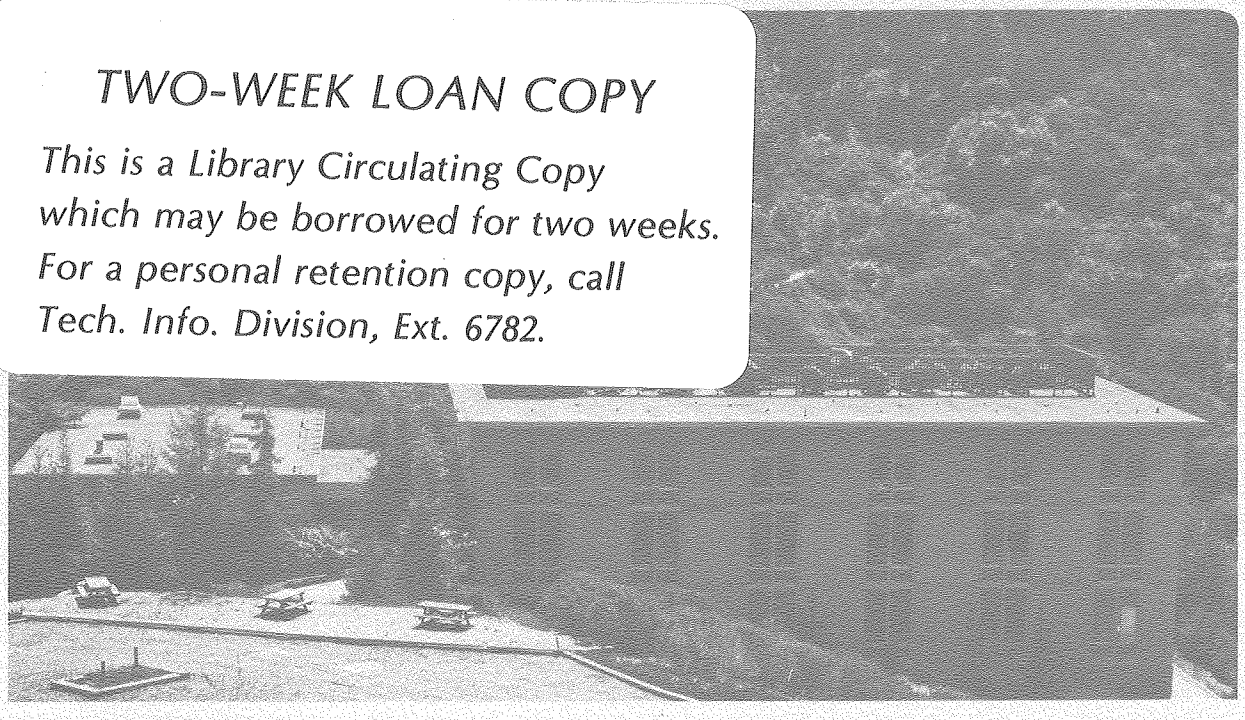

Prepared for the U.S. Department of Energy under Contract W-7405-ENG-48

DISCLAIMER

LBL-11817

INTERPRETATION OF TRACER SURFACE DIFFUSION EXPERIMENTS ON UO_2

ROLES OF GAS AND SOLID TRANSPORT PROCESSES

BY D.R.OLANDER

MATERIALS AND MOLECULAR RESEARCH DIVISION OF THE LAWRENCE BERKELEY LABORATORY AND THE DEPARTMENT OF NUCLEAR ENGINEERING OF THE UNIVERSITY OF CALIFORNIA, BERKELEY, CALIFORNIA 94720, U.S.A.

A B S T R A C T

The spreading of a tracer from an enriched needle source which contacts the surface of a depleted pellet sink is analyzed rigorously. It is shown that volume diffusion in both the needle and the pellet need to be considered because only by this process is sufficient radioactivity accumulated for measurement after the anneal. Parasitic gas phase processes are of two types-evaporative loss of solid if a flowing gas is used, or molecular diffusion from enriched portions of the surface to depleted zones if the couple is in a closed vessel with a stagnant gas. A complete numerical solution including surface diffusion, solid diffusion, evaporative loss and contact resistance is applied to the UO_2 tracer study of Marlowe and Kazanoff at 1915° C. Based upon UO_2 evaporation experiments, the analysis shows that the evaporative loss effect is not important in these experiments. The UO_2 surface diffusion coefficient deduced from analysis of these data is 0.2 ± 0.1 cm^2/s at 1915° C., which is 10^4 times larger than that predicted by extrapolation of values obtained by mass transfer techniques.

I. - INTRODUCTION.

The coefficient of surface self-diffusion on UO_2 is a key parameter in the processes which affect the behavior of oxide nuclear fuels. Although small fission gas bubbles may not be mobile under normal operating conditions, it is widely believed that in rapid transients gas release is controlled by the motion of these bubbles in the grains. Moreover, their velocity in a temperature gradient is assumed to be governed by the mechanism of surface diffusion, and so the surface diffusivity is an important material property in fuel modeling codes (1 - 3). This quantity can be measured either by tracer techniques or by mass transfer methods (grain boundary grooving or scratch decay). Maiya's experiments using the latter technique (4) indicated that the grain boundary grooving method is totally evaporation controlled on UO_2 for temperatures above 1700°C. Maiya also re-examined earlier grain boundary grooving and scratch decay experiments (5 - 7) and attempted to correct the data for vapor transport, which competes with surface diffusion for temperatures > 1400°C. Not having access to the original data, Maiya was forced to guess certain experimental parameters in order to apply the vapor-transport correction. The equation for the surface diffusion coefficient D_S which resulted from Maiya's compilation has a pre-exponential factor of 5×10^5 cm^2/s and an activation energy of 108 kcal/mole.

The only tracer study of surface diffusion on UO_2 is that of Marlowe and Kazanoff (hereafter denoted by MK) (9), which resulted in a pre-exponential factor 100 times larger and an activation energy 13 kcal/mole greater than those suggested by Maiya. MK interpreted their tracer spreading data in terms of surface diffusion alone - volume diffusion and gas phase transport were claimed to be unimportant. Robertson (8), using a method proposed by Shewmon (10), corrected the MK results at 1915°C. (the only temperature at which the original data were available) and concluded that the correct value of D_S implied by these data is 300 times larger than the value deduced by MK, or more than

.../..

three orders of magnitude larger than the values from the Maiya correlation. Consequently either there is a real physical difference between the mass transfer and tracer methods, or the mathematical interpretation of the MK data is incorrect. In this paper, the latter possibility is examined.

The tracer technique for measuring surface diffusivity utilized by MK is shown in Fig.1. A needle of 93% enriched UO_2 with a flattened point contacted a polished surface of a pellet of depleted UO_2 (0.2 % U-235). After a known contact time at a fixed temperature, the radial distribution of tracer was determined by counting the U-234 alpha activity. The experiment was conducted in flowing hydrogen. No transfer of activity from the needle to the pellet was observed when the two were slightly separated. The needle was not sintered to the pellet after the anneal.

Furaya and Koizumi (11) used the tracer technique to measure surface spreading of Pu-239 on UO_2. The important distinction between this experiment and that of MK was the flow condition of the gas phase. In MK's case, the specimen was immersed in a flowing gas, with a flow rate high enough to prevent isotope transfer from the enriched to the depeleted specimens via the gas phase. However, there undoubtedly was evaporative loss of UO_2 from all surfaces. In Furaya and Koizumi's experiment, on the other hand, the specimen was totally enclosed by a metal crucible. There was no possibility of significant evaporative loss from such an arrangement, but transfer of tracer from the enriched to the depleted surfaces by molecular diffusion in the stagnant gas could and did occur. The effect was very large at high temperature, resulting in a 20-fold decrease in the apparent surface diffusivity when the gas phase transfer process was impeded by masking the depleted surface during an anneal. Not enough information is provided in Ref.11 to analytically estimate the gas phase transfer effect.

Robertson's re-interpretation of the MK data (8) to include bulk diffusion of the tracer is subject to improvement in the following areas :

1. - The Shewmon theory used by Robertson is based on an approximate solution of the mathematical surface mass balances. The accuracy of this approximate solution is unknown.

2. - Data analysis relies only on the slope of log (activity) versus radius plots. The magnitude of the activity, which is equally significant, is ignored.

3. - The theory used in the interpretation assumes a constant tracer concentration at the needle-pellet interface, which is incorrect because the needle surface becomes depleted of tracer as much or more so than the surface of the depleted pellet becomes enriched.

4. - It was assumed that the count rate at any radial location is proportional to the total quantity of tracer which had diffused into the bulk at this point. However, because alpha particles have a range of ~ 10 µm in UO_2, this assumption is incorrect.

5. - On the basis of MK's observation of no activity transfer when the needle and pellet are not in contact, evaporative transfer of tracer from the enriched source to the depleted sink was correctly ruled out. However, evaporative loss of UO_2 from all surfaces into the flowing hydrogen could affect both the surface and bulk diffusion processes.

6. - The possibility of a transfer resistance at the point of contact between the needle and the pellet was not considered. Such a resistance is common in diffusion couples used in volume diffusion experiments, and there is no reason to ignore it in a surface diffusion couple.

Items 1 - 4 of this list can be accounted for analytically. The last two items, however, each involve a distinct physical process which must be added to the mathematical model. It is therefore important to estimate the magnitudes of the parameters which characterize these parasitic processes in the overall transport process. Such parameters must

either be determined independently or in the course of fitting the tracer spreading data to the theory, a procedure which necessarily reduces the accuracy of the values of surface diffusivity which can be deduced from the data. In order to alleviate such data-fitting problems, experiments were performed to provide information on the magnitude of the evaporative loss effect to be expected in the MK system.

II. - UO_2 VAPORIZATION EXPERIMENTS.

UO_2 specimens were vaporized in flowing gas streams at atmospheric pressure. As shown in Fig.2, samples in the form of disks 1 mm thick and 1.2 cm in diameter are suspended from the arm of an electrobalance by a rhenium wire. The gas is fed into the bottom of a tungsten crucible and flows upward. The crucible is mounted in a vacuum resistance furnace and the temperature is measured by a tungsten-rhenium thermocouple touching the outside wall of the crucible. In auxillary experiments using an inside thermocouple as well as the outside one, the outside thermocouple was calibrated in terms of the internal temperature. Weight losses were recorded as a function of time at various temperatures and flow rates of either argon or hydrogen. Only evaporation occurs in argon, but the weight loss rate in hydrogen is the sum of evaporation and reduction. Only the evaporative component is of interest here.

In convective mass transfer experiments of the type described above, the rate of vaporization is governed by the mass transfer coefficient according to the following equation :

$$J_{evap} = k(C_g - C_{bulk}) \qquad (1)$$

where J_{evap} is the rate of evaporation per unit surface area in moles/cm^2-s, k is the mass transfer coefficient in cm/s, and C_g is the saturation concentration of solid in the gas at the surface, as obtained from the vapor pressure of UO_2. Actually, the vapor pressure used to

compute the driving force for evaporation should be the sum of the pressures of all uranium-bearing gaseous species in equilibrium with the surface of the specimen . In stoichiometric UO_2, the most volatile species is UO_3, which thus vaporizes preferentially in the early stages of surface recession. The surface becomes depleted by noncongruent vaporization, but ultimitely reaches a steady state substoichiometry dictated by the requirement that the O/U ratio in the evaporating vapor be the same as that of the bulk solid (which is nearly stoichiometric). The total vapor pressure above the substoichiometric surface may be somewhat different than that of stoichiometric UO_2, but this difference is neglected in the present analysis. The partial pressure of UO_2 in the bulk gas, C_{bulk} in Eq(1), is essentially zero because of the small sample size and the high gas flow rates used.

A typical weight-loss curve is shown in Fig.3. During the initial period of argon flow, the specimen weight decreases linearly with time. The slope is a direct measure of the flux J_{evap} and Eq (1) can be used to determine the mass transfer coefficient k. The weight loss rate increases dramatically when the gas is switched to hydrogen, but most of the increase is due to reduction of the sample. In order to rationalize the pure evaporation data obtained in argon and to estimate the evaporation contribution in hydrogen, the mass transfer correlation for flow over a flat plate was used (12) :

$$Sh = 0.664\ Sc^{1/3} Re^{1/2} \qquad (2)$$

where

$$Sh = k\ell/D_g$$

is the Sherwood number,

$$Sc = \nu/D_g$$

is the Schmidt number, and

$$Re = v\ell/\nu$$

is the Reynolds number. In these equations, ℓ is the downstream distance from the leading edge of the flat plate and is taken as the mean

chord length of the flat surface of the disks used in the present experiment. D_g is the diffusivity of UO_2 in the gas as calculated from kinetic theory, and ν is the kinematic viscosity of the gas. v is the free-stream velocity of the gas obtained from the volumetric flow rate and the cross sectional area of the crucible in which the samples are hung. Although the arrangement of Fig.2 does not correspond to a classical flat plate experiment, this idealized geometry is the closest representation of the actual convective transfer conditions.

Experiments were conducted at 1900°C. with free stream gas velocities of 9, 11 and 22 cm/s. One experiment was made at 2000°C. at a gas velocity of 23 cm/s. These conditions produced weight-loss rates which varied by a factor of five. When converted to mass transfer coefficients and plotted in the manner suggested by Eq (2), the data appear as shown in Fig.4. They follow the predicted flow rate effect quite accurately. The data for the two temperatures investigated fall on the same line, which means that the data are consistent with the vapor pressure-temperature relation used to deduce mass transfer coefficients from evaporation fluxes according to Eq (1).

The data follow the form of Eq (2) except that the numerical coefficient for the former is six times larger than predicted by flat plate theory. This is believed to be due in part to edge effects in the experiment and to failure of the suspended disk to behave as an ideal flat plate. In addition, if the samples were slightly hyperstoichiometric, vaporization of UO_3 would significantly enhance the vapor pressure and hence the evaporation rate. However, the argon data are sufficient to permit a reasonably accurate extrapolation to the vaporization in hydrogen. This extrapolation was made using Eq (2) and the values of the transport properties (i.e., D_g and ν) of the two gases. This procedure resulted in a predicted mass transfer coefficient in hydrogen which is 2.1 times larger than in argon, hence the origin of the dashed line marked "expected H_2 evaporation" in Fig.3.

Instead of expressing UO_2 vaporization by a mass transfer coefficient, it is convenient to employ the surface recession velocity $V = J_{evap}/C_v$, where $C_v = 0.041$ moles/cm^3 is the molar density of solid UO_2. Using

Eq (1) for J_{evap} (C_{bulk} being zero), we have :

$$V = kC_g/C_v \qquad (3)$$

Using the experimental mass transfer coefficients in argon, the surface recession velocities computed from Eq (3) are multiplied by 2.1 to obtain the expected values in hydrogen. This calculation yields V = 1.0 µm/hr at 1915°C for a gas flow velocity of 22 cm/s. Since the flow velocities used in the evaporation experiments were deliberately high to emphasize the vaporization process, we expect the UO_2 vaporization rate in the MK experiments to be less than 1 µm/hr.

III. - ANALYSIS OF THE MK TRACER EXPERIMENT.

Having at least placed an upper limit on the rate of evaporation of UO_2, analysis of the MK tracer diffusion system involves two unknown parameters, the surface diffusion coefficient and the contact resistance between the needle and the pellet. The bulk diffusion coefficient of U in UO_2, having been measured in a number of independent experiments, is assumed to be known. However, even for nominally stoichiometric UO_2 there is a spread of about a factor of 5 at 1900°C., and the use of hydrogen in the MK experiment means that the UO_2 is probably not stoichiometric. That this transport property is indispensable to the understanding of the tracer diffusion process is clear ; it is only by virtue of diffusion of tracer atoms into the bulk of the pellet that a detectable alpha count rate is attainable. If the process involved only transport of tracer atoms in the topmost atomic layer of the surface and if this layer were fully enriched, the detected activity would be equivalent to that from a bulk solid uniformly enriched to ~ 0.006 %. Or, if the volume diffusion coefficient were zero, the tracer experiment would detect no alpha -radiation no matter what the mobility of molecules of UO_2 on the surface.

The concept, often used in surface diffusion analyses, of a "high diffusivity layer" many atomic distances thick must also be rejected. Enough is known about crystal surfaces, including those of ceramics such as UO_2

to state that the bulk crystal structure persists to the surface, with at most a slight relaxation or reconstruction of the surface plane of atoms (13). The surface must be treated mathematically as a plane terminating the bulk structure on which lateral atom motion occurs by movement of molecules across terraces from temporary binding sites such as kinks and ledges. The mass balance equation in which surface diffusion appears conserves the areal density of tracer atoms. On the surface of the depleted pellet denoted as region 1 in Fig.1, the balance is :

$$\frac{\partial C_S^+}{\partial t} = D_s \frac{1}{r} \frac{\partial}{\partial r}\left(r \frac{\partial C_s^+}{\partial r}\right) + D_V \left(\frac{\partial C_V^+}{\partial z}\right)_{z=0} + \left(\frac{\partial C_s^+}{\partial t}\right)_{evap} \qquad (4)$$

where C_s^+ is the number of gram atoms of tracer per unit area of exposed surface and D_s is the surface diffusion coefficient. Radial location is denoted by r and z is the depth of penetration into the solid. C_V^+ is the molar volumetric concentration of tracer atoms at depth z and D_V is the volume self diffusion coefficient of uranium ions in polycrystalline UO_2. In this equation, the second term on the right hand side represents loss of tracer atoms from the surface by volume diffusion into the solid and the last term reflects the contribution due to evaporation. The surface and volume diffusion terms represent interchanges of tracer and normal atoms or molecules and hence do not produce changes in the total concentration of surface atoms. The evaporative term, on the other hand, removes both tracer and normal uranium atoms at rates proportional to their surface concentrations. This term is nonzero only if there is a bulk concentration gradient ; if the concentration is uniform in the solid, evaporation does not change the concentration of tracer atoms on the surface. Suppose, however, that the surface recedes by evaporation with a velocity V and the bulk enrichment is a known function of depth, q(z). In a time Δt, the concentration of tracer on the exposed surface changes by :

$$\Delta C^+_s = C_s \left[q(\Delta z) - q(0) \right] \simeq C_s \left(\frac{\partial q}{\partial z}\right)_{z=0} \Delta z$$

where C_s is the total number of uranium atoms per unit of surface area, which for the low-index planes of UO_2 is 1.1×10^{-9} g. atoms U/cm^2. Since $\Delta z = V \Delta t$, the evaporation term in Eq (4) is :

$$\left(\frac{\partial C_s^+}{\partial t}\right)_{evap} = \frac{\Delta C_s^+}{\Delta t} = C_s V \left(\frac{\partial q}{\partial z}\right)_{z=0} \tag{5}$$

the surface and bulk enrichments are defined by :

$$\begin{aligned} q_s &= C_s^+/C_s \\ q &= C_v^+/C_v \end{aligned} \tag{6}$$

Normalized surface and bulk concentrations are defined by :

$$\begin{aligned} u_1 &= \frac{q_s - q_D}{q_E - q_D} \\ v &= \frac{q - q_D}{q_E - q_D} \end{aligned} \tag{7}$$

where q_E and q_D are the original tracer fractions in the enriched needle and in the depleted pellet, respectively. Because the tracer enrichments are continuous at the interface, u_1 is equal to the value of v at $z = 0$.

Dimensionless time, distance and property parameters are given by :

$$\begin{aligned} \tau &= \frac{D_v t}{z_F^2} \\ \eta &= r/b \\ Z &= z/z_F \\ E &= \frac{1}{\sqrt{\pi}} \frac{b^2}{z_F} \frac{D_v C_v}{D_s C_s} \\ G &= \frac{\sqrt{\pi} C_s}{z_F C_v} \\ A &= \frac{V z_F}{D_v} \end{aligned} \tag{8}$$

where b is the radius of the point of the needle contacting the pellet surface and z_F is the range of the tracer alpha particles in UO_2.

Inserting Eqs (5) - (8) into Eq (4) yields :

$$EG \frac{\partial u_1}{\partial \tau} = \frac{1}{\eta} \frac{\partial}{\partial \eta} \left(\eta \frac{\partial u_1}{\partial \eta} \right) + \sqrt{\pi}\, E \left(1 + \frac{AG}{\sqrt{\pi}} \right) \left(\frac{\partial v}{\partial Z} \right)_Z = 0 \qquad (9)$$

Evaluation of the gradient in the last terms on the right hand side requires analysis of tracer transport in the solid. The experiments of Chilton and Edwards(14) demonstrated that migration of heavy metals in polycrystalline UO_2 of the type used in the MK experiments occurs primarily by grain boundary diffusion. However, in interpreting their penetration data, these authors did not use the analysis which explicitly recognizes distinct grain boundary and lattice transport mechanisms(15). Rather, they used the Boltzmann-Montano method to determine effective homogeneous-medium diffusivities from the data. Because of the influence of grain boundary diffusion, the values of D_V so deduced are much larger than those representing true lattice cation diffusion. Although the values of D_V reported by Chilton and Edwards represent a blend of lattice and grain boundary diffusion, the effective diffusivities can only be used in the same framework as the one from which they were obtained, namely in conjunction with a conservation statement appropriate to a homogeneous medium. Thus, the equation which must be used if bulk penetration is to be described by Chilton and Edwards' diffusion coefficients is Fick's second law.

Because the bulk diffusivity is small, diffusion parallel to the surface (i.e., in the r-direction) can be neglected. As will be seen later, the penetration depth of tracer perpendicular to the pellet surface is ~ 10μm. Radial transport by solid state diffusion must be even smaller because the

diffusion geometry is cylindrical rather than axial. Consequently, tracer detected at radii from a 1 to 5 mm cannot possibly reflect transport by solid state diffusion in the radial direction. The same conclusion follows from the analysis of Ref. 10.

Because of surface evaporation, we must deal with a moving-boundary problem. With z = 0 located at the moving surface, the diffusion equation for the tracer in the bulk is:

$$\frac{\partial C_v^+}{\partial t} - V \frac{\partial C_v^+}{\partial z} = D_v \frac{\partial^2 C_v^+}{\partial z^2} \tag{10}$$

or, in dimensionless terms,

$$\frac{\partial v}{\partial \tau} - A \frac{\partial v}{\partial Z} = \frac{\partial^2 v}{\partial Z^2}$$

The boundary and initial conditions are :

$$v\ (Z,0) = 0 \tag{11a}$$

$$v\ (0,\tau) = u_1\ (\eta,\tau) \tag{11b}$$

$$v\ (\infty,\tau) = 0 \tag{11c}$$

Using Duhamel's theorem (16), the solution is :

$$v = \int_0^\tau u_1\ (\eta,\tau)\ \frac{\partial}{\partial \tau}\ g\ (Z,\tau - \lambda)\ d\lambda \tag{12}$$

.../..

where g (Z,τ) is the solution of Eqs (10) and (11) with the condition of Eq (11b) replaced by g (0,τ) = 1. This solution is [16] :

$$g\ (Z,\tau) = \frac{1}{2}\left\{ \operatorname{erfc}\left(\frac{Z + A\tau}{2\sqrt{\tau}}\right) + e^{-AZ}\operatorname{erfc}\left(\frac{Z - A\tau}{2\sqrt{\tau}}\right)\right\} \tag{13}$$

Substituting Eq (13) into Eq (12) yields :

$$v = \frac{2}{\sqrt{\pi}} \int_{\frac{Z}{2\sqrt{\tau}}}^{\infty} u_1\ \left(\eta,\tau - \frac{Z^2}{4X^2}\right)\ \exp\left[-\left(X + \frac{AZ}{4X}\right)^2\right] dX \tag{14}$$

Since we are only interested in the behavior of v as Z → 0 (i.e., in $(\partial v/\partial Z)_{Z = 0}$), the u_1 - function in Eq (14) can with acceptable accuracy be expanded in a two-term Taylor series :

$$u_1\left(\eta,\tau - \frac{Z^2}{4X^2}\right) = u_1\ (\eta,\tau) - \left(\frac{Z^2}{4X^2}\right)\frac{\partial u_1}{\partial \tau} \tag{15}$$

Comparison with the analytical solutions for A = 0 (16) shows that use of this approximation in Eq (14) is exact for u_1 = constant and for $u_1 \propto \tau$, and is within 1 % of the exact solution for $u_1 \propto \sqrt{\tau}$.

Substituting Eq (15) into Eq (14), performing the required integrations and taking the derivative at Z = 0 yields :

$$\left(\frac{\partial v}{\partial Z}\right)_{Z = 0} = -\frac{F_1\ (y)}{\sqrt{\pi\tau}}\ u_1\ (\eta,\tau) - \sqrt{\frac{\tau}{\pi}}\ F_2\ (y)\ \frac{\partial u_1}{\partial \tau} \tag{16}$$

where :

$$F_1\ (y) = e^{-y^2} + \sqrt{\pi}\ y\left[1 + \operatorname{erf}(y)\right] \tag{17a}$$

$$F_2\ (y) = \frac{\sqrt{\pi}}{2}\frac{\operatorname{erf}(y)}{y} \tag{17b}$$

.../..

and :

$$y = \frac{1}{2} A \sqrt{\tau} \qquad (18)$$

Surface evaporation enters via the $AG/\sqrt{\pi}$ term of Eq (9) and in the F_1 and F_2 functions in Eq (16). The former is :

$$\frac{AG}{\sqrt{\pi}} = \frac{VC_s}{D_v C_v}$$

and the parameter y is :

$$y = \frac{V\sqrt{t}}{2\sqrt{D_v}}$$

From the compilation of Chilton and Edwards (14), the smallest expected value of D_v is ~ 1.5×10^{-11} cm^2/s at 1915°C. From the experiments described in Sect. II, the maximum value of V expected in the MK experiments is 1 μm/hr. With $C_s/C_v = 2.7 \times 10^{-8}$ cm, the maximum possible value of $AG/\sqrt{\pi}$ is ~ 5×10^{-5}, which can clearly be neglected compared to unity in Eq (9). For the 20-minute anneal at 1915°C in the MK work, the maximum value of y is 0.13, for which $F_1 = 1.25$ and $F_2 = 1.00$. These are sufficiently close to the limits at $y = 0$ ($F_1 = F_2 = 1$) that to a good approximation, the effect of vaporization in the MK experiments is small. However, the moving boundary effect on bulk diffusion (i.e., the F_1 and F_2 functions in Eq (16)) is retained in the analysis.

Neglecting $AG/\sqrt{\pi}$ compared to unity and substituting Eq (16) into Eq (9) yields :

$$E\left[\sqrt{\tau} F_2(y) + G\right]\frac{\partial u_1}{\partial \tau} = \frac{1}{\eta}\frac{\partial}{\partial \eta}\left(\eta \frac{\partial u_1}{\partial \eta}\right) - E\frac{F_1(y)}{\sqrt{\tau}} u_1 \qquad (19)$$

The parameter G in this surface balance equation is negligible except near $\tau = 0$. Numerical solution of this equation verifies that G can be dropped from the equation without significant effect on the computed concentration profiles. Neglecting G in Eq (19) is equivalent to setting the left hand side of Eq (4) equal to zero, which signifies that the surface layer has a negligible capacity for storing tracer atoms (compared to the capacity of the bulk).

With the parameter G absent from the equations, the surface diffusivity enters the analysis only in the product $D_s C_s$. Determination of D_s alone requires specification of the total areal density of atoms, which depends upon the surface plane exposed. However, separate values of C_s and D_s are never needed in any practical application of the surface diffusion process. In the theory of temperature gradient migration of gas bubbles in solids by the surface diffusion mechanism, for example (17), only the product $D_s C_s$ is required. Concern over the thickness of a high diffusivity surface layer is a fiction, one which makes no physical sense and which, moreover, is not needed to apply basic surface mobility measurements to practical situations.

Equation (19) provides a single partial differential equation which, if supplied with appropriate boundary conditions, could be solved for the surface enrichment profile as a function of time, $u_1(\eta,\tau)$. Previous treatments of tracer diffusion experiments (e.g., Ref.10) applied a condition of constant enrichment at the needle-pellet contact circle, which is equivalent to setting $u_1(1,\tau) = 1$ and implies that the bulk tracer concentration of the enriched source is maintained at this point for all times. However, the enriched needle is microstructurally identical to the depleted pellet, and if the transport of tracer atoms in the latter is determined by surface diffusion, bulk diffusion, and evaporation, the same must be true of the former. The existence of the same transport resistances in the source needle as in the pellet sink means that the needle must be modeled in the same manner as the pellet. Therefore, we write surface mass balances for the needle which, by the geometry depicted in Fig.1, is divided into two regions. Region 2 is the conical surface extending from the pellet-needle contact circle to the beginning of the cylindrical portion, which is denoted as region 3. The analysis of transport on regions 2 and 3 is the same as that just described for region 1 except that the right hand sides of Eqs (11a) and (11c) are 1 instead of 0. With this change, the surface mass balances for the needle zones are :

$$E\left[\sqrt{\tau}F_2(y) + G\right]\frac{\partial u_2}{\partial \tau} = \frac{1}{\mu}\frac{\partial}{\partial \mu}\left(\mu \frac{\partial u_2}{\partial \mu}\right) + E\frac{F_1(y)}{\sqrt{\tau}}(1 - u_2) \qquad (20)$$

.../..

and :

$$E\left[\sqrt{\tau}F_2(y) + G\right]\frac{\partial u_3}{\partial \tau} = \frac{\partial^2 u_3}{\partial \xi^2} + E\,\frac{F_1(y)}{\sqrt{\tau}}\,(1 - u_3) \qquad (21)$$

where $\mu = r'/b$ is the radial distance along the cone measured from the hypothetical cone tip and $\xi = z'/b$ is the axial distance along the cylindrical portion of the needle measured from the intersection of the conical and cylindrical surfaces.

The initial conditions in the three regions of the diffusion couple are :

$$\begin{aligned} u_1(\eta,0) &= 0 \\ u_2(\mu,0) &= 1 \\ u_3(\xi,0) &= 1 \end{aligned} \qquad (22)$$

and the boundary conditions are as follows. The pellet is assumed to be an infinite half-solid, so :

$$u_1(\infty,\tau) = 0 \qquad (23)$$

The needle-pellet contact circle is at $\eta = 1$ or $\mu = \csc\phi$, where 2ϕ is the angle at which the needle was sharpened. At this contact circle, the flux matching condition is :

$$-\left(\frac{\partial u_1}{\partial \eta}\right)_{\eta = 1} = H\left[u_2(\csc\phi,\tau) - u_1(1,\tau)\right] \qquad (24)$$

where H is a dimensionless contact resistance parameter which can only be determined by fitting the theory to the data. Equality of the surface fluxes of tracer atoms on either side of the contact circle also requires that :

$$-\left(\frac{\partial u_1}{\partial \eta}\right)_{\eta = 1} = \left(\frac{\partial u_2}{\partial \mu}\right)_{\mu = \csc\phi} \qquad (25)$$

From the geometry of the needle source reported by MK, the junction between regions 2 and 3 occurs at $\mu = 8\csc\phi$ which is equivalent to $\xi = 0$. Since there is no contact resistance at this junction, we have :

$$u_2(8\csc\phi,\tau) = u_3(0,\tau) \tag{26}$$

and :

$$\left(\frac{\partial u_2}{\partial \mu}\right)_{\mu = 8\csc\phi} = \left(\frac{\partial u_3}{\partial \xi}\right)_{\xi = 0} \tag{27}$$

Assuming the cylindrical portion of the needle to be infinitely long yields the final boundary condition :

$$u_3(\infty,\tau) = 1 \tag{28}$$

Solutions of Eqs (19), (20) and (21) subject to the initial conditions of Eq (22) and the boundary and matching conditions given by Eqs (23) - (28) determines $u_1(\eta,\tau)$ for specified values of the needle angle 2ϕ, the surface diffusion parameter E, the contact resistance parameter H, and the evaporation parameter A. However, the experiment does not measure u_1; rather, it determines the decay rate of alpha particles crossing the surface of the depleted pellet from tracer atoms which have diffused into the bulk. At radius r and depth z beneath the depleted surface, the source strength of alpha particles in $\lambda C_v q(r,z,t)$, where λ is the decay constant of the tracer. The current I at the surface due to this distributed volumetric source is (17):

$$I = \frac{1}{2}\int_0^{Z_F} \lambda C_v q(r,z,t)(1 - z/z_F)dz \tag{29}$$

where z_F is the range in UO_2 of the alpha particles from the decay of tracer atoms. The activity detected in the MK experiment (after correction to a per unit area basis) is proportional to the current I of Eq (29). Using $q = q_E$ in this equation, the activity of the enriched source is proportional to :

$$I_E = \frac{1}{4} \lambda C_v z_F q_E \tag{30a}$$

and that for the depleted material is :

$$I_D = \frac{1}{4} \lambda C_v z_F q_D \tag{30b}$$

A dimensionless activity R, which is obtainable from the experimental data as well as from the theory, is defined by :

$$R(\eta,\tau) = \frac{I - I_D}{I_E - I_D} = 2 \int_0^1 v(\eta,\tau,Z)(1 - Z)dZ \tag{31}$$

Substituting Eq (14) into Eq (31) yields :

$$R(\eta,\tau) = \frac{4}{\sqrt{\pi}} \int_0^1 (1 - Z) \int_{\frac{Z}{2\sqrt{\tau}}}^{\infty} u_1\left(\eta,\tau - \frac{Z^2}{4X^2}\right) \exp\left[-\left(X + \frac{AZ}{4X}\right)^2\right] dX\, dZ \tag{32}$$

The experimentally accessible quantity $R(\eta,\tau)$ follows from the solution for $u_1(\eta,\tau)$ by application of the double integration indicated above (without using the approximation for u_1 given by Eq (15)).

IV. - RESULTS AND DISCUSSION.

The experiment of Marlowe and Kazanoff (9) at 1915° C is the only one for which the radial distribution of the alpha particle counting rate on the surface of the initially depleted pellet was reported. Figure 4 of the MK paper gives the activity per unit area, less that of the initial depleted specimen, as a function of radius. These data are proportional to the numerator $I - I_D$ in the quantity R of Eq (31). MK reported that the activity of the enriched material was 142 times greater than that of the depleted UO_2, for which a counting rate of 3.1 was given. The data of MK's Fig.4 were converted to R values by dividing each point by 142 x 3.1 - 3.1 = 437.

The geometry of the MK specimen was completely reported except for the angle at which the enriched needle was shaped. We have made numerical tests with the full cone angle of Fig.1 (i.e., 2ϕ) equal to 30° and 45°. The needle trip radius was given in Ref. 9 as b = 0.01 cm. so that radial position on the pellet surface can be converted to the dimensionless quantity η. Conversion of the experimental annealing time (20 min) to the dimensionless time τ requires knowledge of the alpha particle range z_F and the bulk diffusivity of uranium in UO_2, D_v. The range of the 5.5 MeV alpha particles from decay of Pu-239 is reported to be 11.7 μm (18). Hawkins and Alcock (19) cite a range of 10.2 μm for the 4.82 MeV alpha particle from U-233 in UO_2 and Hirsch and Matzke (20) use a range of 10 μm for the 4.77 MeV U-234 alpha particle in UO_2. We adopt this value for the present calculations.

Chilton and Edwards (14) have measured the penetration of Pu in UO_2, which occurs via grain boundaries. Based upon these results and their correlation of earlier data, D_v is estimated to lie between 1.5×10^{-11} and 7.5×10^{-11} cm^2/s at 1915° C. It should be noted that this range of values applies to material which is nominally stoichiometric whereas the urania in the MK experiment is probably hypostoichiometric because hydrogen was used as the cover gas. Based upon these two extreme values of D_v, the dimensionless time in the MK experiment is probably between 0.018 and 0.090.

The surface spreading data of Ref.9 were fitted to the theory for four specified combinations of needle cone angle and dimensionless time. For each of the four cases, the experimental data in the form of dimensionless alpha activity R versus dimensionless radius η were fitted to the theory by choosing values of the surface diffusivity parameter E and the contact resistance parameter H. The evaporation parameter A was set equal to zero. The results are shown on Fig.5 and the corresponding parameters of the best fits are given in Table 1.

.../..

Except for the radial location closest to the enriched needle, Fig.5 demonstrates satisfactory fitting of the model to the experimental results. The data point at $\eta = 10 (r = 1$ mm) is subject to the largest experimental error, particularly since the aperature counting technique requires both the value of the countrate for a circular area of radius r and its derivative (9). Using the maximum error indicated by MK for their integral countrate data, the point at $\eta = 10$ on Fig.5 is subject to an error of ~ 15 %. For the maximum value of this range, the data point in question would fall ~ 10 % below the predictions of 3 of the 4 cases treated by the theory. The fit of the theory to the data is well within the uncertainty of the latter for the remaining points.

Use of the contact resistance H as a fitting parameter is essential to obtaining the accord shown in Fig.5. With $H = \infty$ (i.e., perfect contact at the needle-pellet interface), the data point at $\eta = 10$ in Fig.5 would be a factor of two below the predictions which fit the remaining points adequately. However, the values of the surface diffusion parameter E corresponding to these (poorer) fits are close to the values shown in Table 1.

Based upon the values of the parameter E given in the fourth column of Table 1, the product $D_s C_s$ can be calculated from the definition of E (Eq (8)). Taking C_s to be the average areal density of uranium ions on the (100), (110) and (111) planes of the UO_2 crystal structure, the surface diffusion coefficients shown in the last column of Table 1 are deduced. The uncertainties in the needle cone angle and in the volume diffusivity result in a factor of ~ 2 spread in the values of D_s deduced from the data. Data fitting with $D_v = 7.5 \times 10^{-11}$ cm^2/s produces a surface diffusity of 0.22 ± 0.04 cm^2/s, although the fits are not as good as those in which D_v is taken to be 1.5×10^{-11} cm^2/s, for which D_s is found to be 0.13 cm^2/s. These results show that a factor of 5 change in the assumed value of D_v produces only a factor of 1.7 change in the value of D_s extracted from the data. However, even the smaller value of $D_s = 0.13$ cm^2/s is ~ 3000 times larger than the value deduced by MK from the same data. It is also $> 10^4$ times larger than the value obtained from Maiya's correlation (4).

Figure 6 illustrates the effect of surface evaporation on radial spreading of the tracer. This plot shows theoretical curves corresponding to the parameters of case 3 in Table 1, in one instance with no evaporation and in the other with the maximum expected surface recession velocity of 1 μm/hr (see Sect.II). Nonzero values of the evaporation parameter, A, lower the surface spreading curve by nearly a constant fraction, which is roughly the same effect caused by an increase in the parameter E. If the theory had been fitted to the data assuming the maximum evaporation rate (i.e., with A = 2 for cases 1 and 3 and A = 0.4 for cases 2 and 4), the same quality of fit seen in Fig. 5 would be obtained but the surface diffusivities deduced from the fitting procedure would have been ∿ 30% larger than the values shown in Table 1. This relatively small effect of evaporation is understandable. Tracer penetration into the bulk solid follows roughly the function erfc $(z/Z\sqrt{D_V t})$ (viz., Eq. (13) with A = D). The complementary error function is essentially zero for an argument of ∿ 2, which gives a penetration depth of $4\sqrt{D_V t}$. For MK's 20 minute experiment at 1915°C, the range of volume diffusivities at this temperature, the tracer penetration depth is 5 to 12 μm. For a surface recession velocity of 1 μm/hr, surface removal in the same time period, Vt, is 0.3 μm, which is quite a bit smaller than the tracer penetration depth. Thus, even allowing for the most severe evaporation rate, the effect on D_S is less than the effect due to the uncertainty in the volume diffusion coefficient.

Finally, Fig.6 compares the prediction of the present numerical procedure with the analytic approximation due to Shewmon (10). The latter yields an analytical formula for the bulk tracer concentration as a function of r, z and t, which when converted to the dimensionless form $v(\eta,\tau,Z)$ and inserted into Eq (31) yields :

$$R(\eta,\tau) = \frac{2}{\sqrt{\pi}}\sqrt{\tau}f(\tau)\,K_0\left(\frac{\sqrt{E}}{\tau^{1/4}}\,\eta\right)\Big/K_0\left(\frac{\sqrt{E}}{\tau^{1/4}}\right) \qquad (33)$$

where E, τ, and η have the same meanings as in the present study. In Eq (33), K_0 is the modified Bessel function of order zero and the function f(τ) is :

$$f(\tau) = 2 - 2\sqrt{\pi}\;\mathrm{ierfc}(x) - \frac{\sqrt{\pi}}{2}\frac{\mathrm{erf}(x)}{x} + e^{-x^2} \qquad (34)$$

with $x = 0.5/\sqrt{\tau}$. ierfc is the first integral of the complementary error function (14). Shewmon's solution does not include the effects of contact resistance or depletion of the source needle. Using the E and τ values for case 3 in Eqs (33) and (34) produces the upper curve in Fig.6, which, as expected from the phenomena which have been neglected in its development, gives very much larger predictions of surface spreading than the numerical model described here. Consequently, Shewmon's approximation cannot be generally used for interpretation of tracer surface diffusion data.

Finally, the values of $D_s\delta$ for three analyses of the MK 1915°C data can be compared. Robertson's(8) use of Shewmon's method yields 0.8×10^{-9} cm^3/s; Berman's numerical treatment(21), which in effect avoids the mathematical approximations of the Shewmon theory, yields 1.9×10^{-9} cm^3/s; the value from the present work, in which the depth of the "surface layer"(δ) is C_s/C_v, gives 3.5×10^{-9} cm^3/s. Each improvement of the mathematical interpretation of the MK data doubles the deduced surface diffusivity. If the surface layer thickness is taken to be 2.7 Å (equal to C_s/C_v for UO_2), the corresponding surface diffusion coefficients are 0.03, 0.07, and 0.13 cm^2/s, respectively. These values are so large that they cannot be associated with an appreciable activation energy. They are, in fact, approaching typical values of gaseous UO_2 diffusion coefficients(17). The MK surface spreading data suggest that UO_2 moves on its own surface at 1915°C like a two-dimensional ideal gas with a scattering mean free path of ~ 1000 Å rather than by a site-to-site hopping process. Unfortunately, the MK data at other temperatures, which if re-analyzed would greatly clarify this difficulty in physical interpretation, are irretrievable.

V - CONCLUSIONS.

An analysis of surface spreading data which utilizes both the magnitude and the radial variation of the tracer countrate has been developed and implemented numerically. Depletion of the tracer source as well as enrichment of the tracer sink are treated by the model. Parasitic effects such as a contact resistance and evaporation are taken into account. Volume diffusion of tracer is an integral part of the process because it alone permits detection of the tracer transported by surface diffusion. However, volume diffusion does not contribute to radial spreading per se.

Application of the analysis method to the only set of surface spreading data on UO_2 in the literature produces a surface diffusion coefficient at 1915° C which is ~ 3000 times larger than that obtained from the same data by the original experimentors and 4 orders of magnitude larger than that obtained by extrapolation of surface diffusivities inferred from mass transfer methods at lower temperatures. The present analysis yields a surface diffusivity between 0.1 and 0.3 cm^2/s at 1915° C. This value is very much larger than those used in current fuel modeling codes whose predictions of fission gas release are very sensitive to the value of the surface diffusivity employed.

There is no obvious explanation of the enormous discrepancy between the tracer and mass transfer methods of measuring D_s, although the latter is suspect on several grounds. This technique is known to be totally evaporation-controlled above 1700° C and correction of the results of lower temperature measurements was done without access to the original data. Moreover, in the mass transfer method, the relaxation of the surface features upon which the technique relies can be due to gaseous diffusion, solid diffusion, or surface diffusion. Experimentally the controlling process is distinguished by the time-dependence of the relaxation, which is $t^{1/4}$ for surface diffusion and $t^{1/3}$ for the two bulk diffusion mechanisms. Such a method of determining rate-controlling processes is tenuous. In the tracer experiments in a flowing gas, surface diffusion is the only possible mechanism for surface spreading. Gas phase transfer is ruled out experimentally. Radial diffusion in

the solid is eliminated by scale arguments. Consequently the radial spreading data of MK's tracer experiment are trustworthy and with proper mathematical interpretation, provide the most reliable UO_2 surface diffusivity measurements available.

ACKNOWLEDGEMENTS.

The author is grateful to the Département de GENIE ISOTOPIQUE at the CEN/SACLAY for their financial support of the computations and to the excellent numerical analysis and programming of Alain VIAULT of the CISI at SACLAY. K. KIM of the UNIVERSITY OF CALIFORNIA at BERKELEY was responsible for the evaporation measurements, and his contribution is acknowledged. The hospitality and support of the Departement d'Etudes des Combustibles a Base de Plutonium of the CEN/FONTENAY-AUX-ROSES is gratefully acknowledged. Publication of this work was supported by the Office of Basic Energy Sciences of the Department of Energy.under Contract W-7405-ENG-48.

Table 1 Parameters of the Best Fits of the Surface Spreading Data of Ref. 9 at 1915°C to theory(Evaporation neglected)

	Specified parameters		fitted parameters		
case No.	needle cone angle, deg	volume diffusivity, cm^2/s	$Ex10^4$	H	$D_s, cm^2/s$ [a]
1	45	$1.5x10^{-11}$	2.5	1.5	0.13
2	45	$7.5x10^{-11}$	8.5	0.5	0.18
3	30	$1.5x10^{-11}$	2.5	3.0	0.13
4	30	$7.5x10^{-11}$	6.0	0.3	0.26

[a] assuming $C_s = 1.1x10^{-9}$ g atoms/cm^2

REFERENCES

1. - J.R. MATTHEWS and M.H. WOOD, J. NUCL. MATER., 84 (1979) 125

2. - J. REST and S.M. GEHL, 5th INTERNAT. CONF. on STRUCTURAL MECHANIS in REACTOR TECHNOLOGY, BERLIN, Germany (1979)

3. - E.E. GRUBER, NUCL. TECHNOL., 35 (1977) 617

4. - P.S. MAIYA, J. NUCL. MATER., 40 (1971) 57

5. - J. HENNEY and J.W.S. JONES, J. MATER. SCI., 3 (1968) 158

6. - I. AMOTO, R.L. COLOMBO and G.C. GRAPPIOLO, SOL. STATE. COMM., 4 (1968) 237

7. - G.L. REYNOLDS, J. NUCL. MATER., 24 (1967) 69

8. - W.M. ROBERTSON, J. NUCl. MATER., 30 (1969) 36

9. - M.O. MARLOWE and A.I. KAZANOFF, J. NUCL. MATER., 25 (1968) 328

10. - P.G. SHEWMON, J. APPL. PHYS., 34 (1963) 755

11. - H. FURUYA and M. KOIZUMI, in THERMODYNAMICS of NUCLEAR MATERIALS, p. 447, IAEA (1974)

12. - H. SCHLICHTING, BOUNDARY LAYER THEORY, 4th Ed., p. 317, McGrawhill (1960)

13. - G.A. SOMORJAI, "PRINCIPLES of SURFACE CHEMISTRY", Prentice-Hall (1972)

14. - G.R. CHILTON and J. EDWARDS, J. NUCL. MATER., 78 (1978) 182

15. - H.S. LEVINE and C.J. MacCALLUM, J. APPL. PHYS. 31 (1960) 595

16. - H.S. CARSLAW and J.C. JAEGER, "CONDUCTION OF HEAT in SOLIDS", 2nd Ed., OXFORD (1959)

17. - D.R. OLANDER, "FUNDAMENTAL ASPECTS OF NUCLEAR REACTOR FUEL ELEMENTS", USERDA (1976)

18. - G.N. HUFFMAN and C.J. KERSHNER, NUCL. APPL. and TECHNOL., 9 (1970) 434

19. - R.J. HAWKINS and C.B. ALCOCK, J. NUCL. MATER., 26 (1968) 122

20. - H.J. HIRSCH and J.J. MATZKE, J. NUCL. MATER., 45 (1972/73) 29

21. - R.M. BERMAN, TRANS. AMER. NUCL. SOC., 12 (1969) 78

FIGURE CAPTIONS

1. - Enriched needle/depleted pellet couple used in surface diffusion measurements by the tracer method (Ref.9)

2. - Apparatus for measuring UO_2 vaporization under controlled gas flow conditions

3. - Weight-loss of UO_2 at 1900° C. in flowing argon and hydrogen with free stream velocities of 22 cm/s

4. - Comparison of UO_2 vaporization rates in flowing argon with predictions of mass transfer from a flat plate

5. - Fitting of MK surface spreading data at 1915° C. for four specified combinations of needle cone angle and volume diffusion coefficient. The parameters E and H which provide the best fits for each case are shown on Table 1. Evaporation has been neglected.

6. - Effect of evaporation on surface spreading for the conditions of case 3 (table 1). The upper curve is the approximate analytical prediction due to Shewmon (10) for the same values of E and τ.

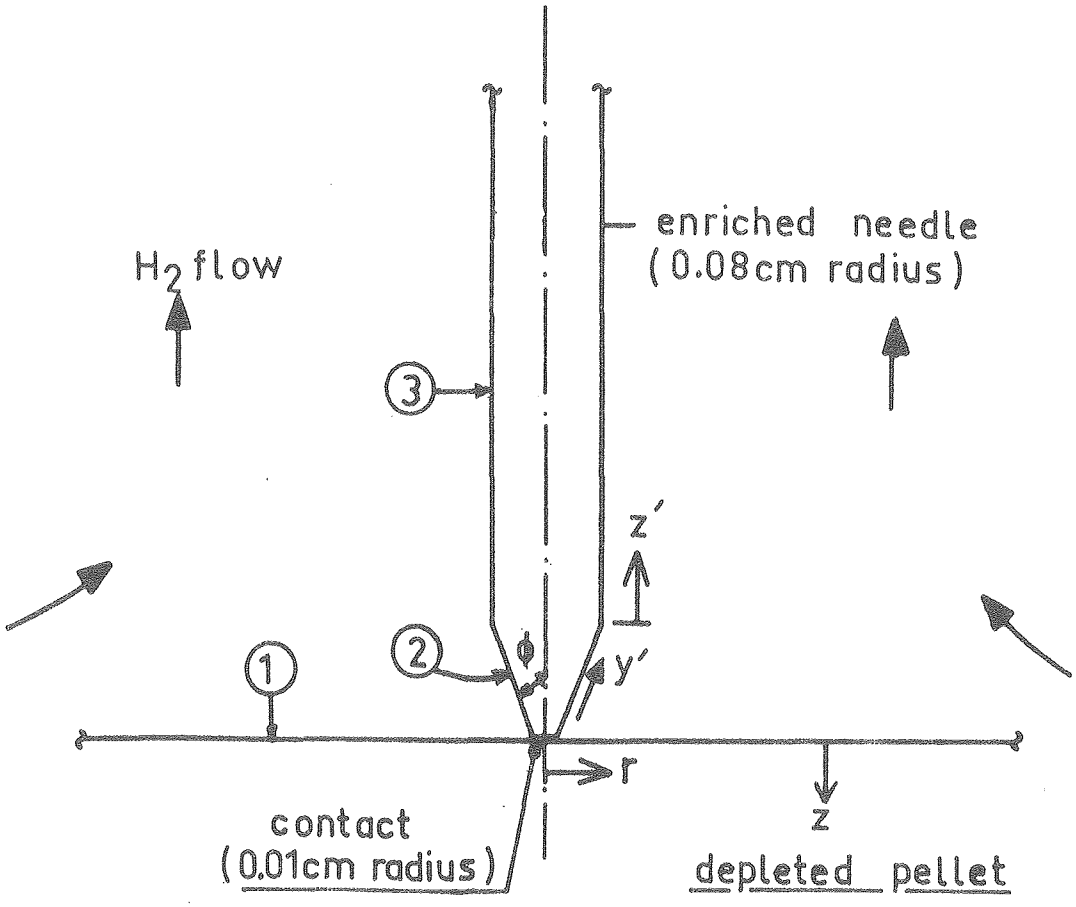
H2 flow
enriched needle
(0.08cm radius)
3
z'
2
1
y'
r
z
contact
(0.01cm radius)
depleted pellet

FIGURE 1

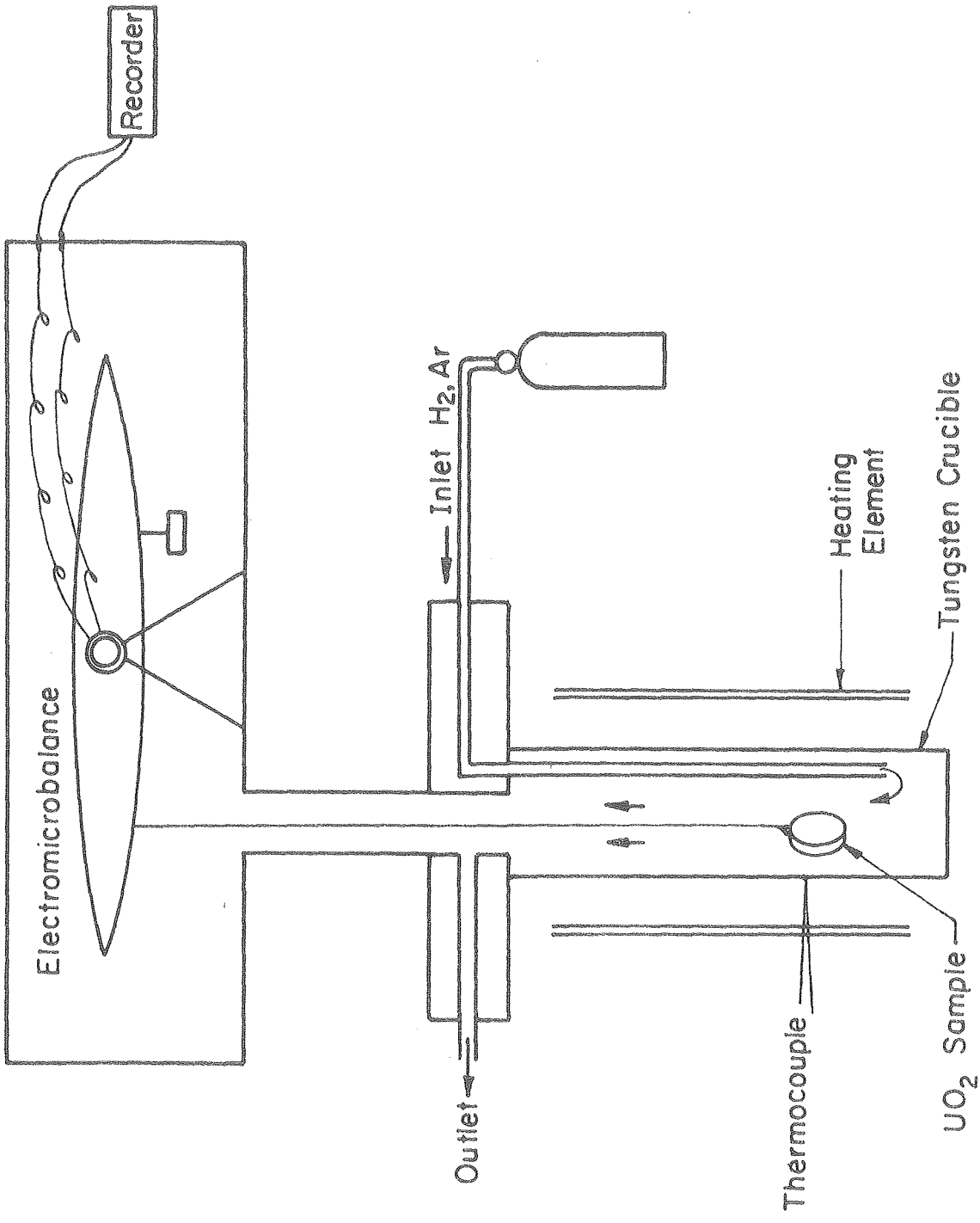

XBL 7712-6571

FIGURE 2

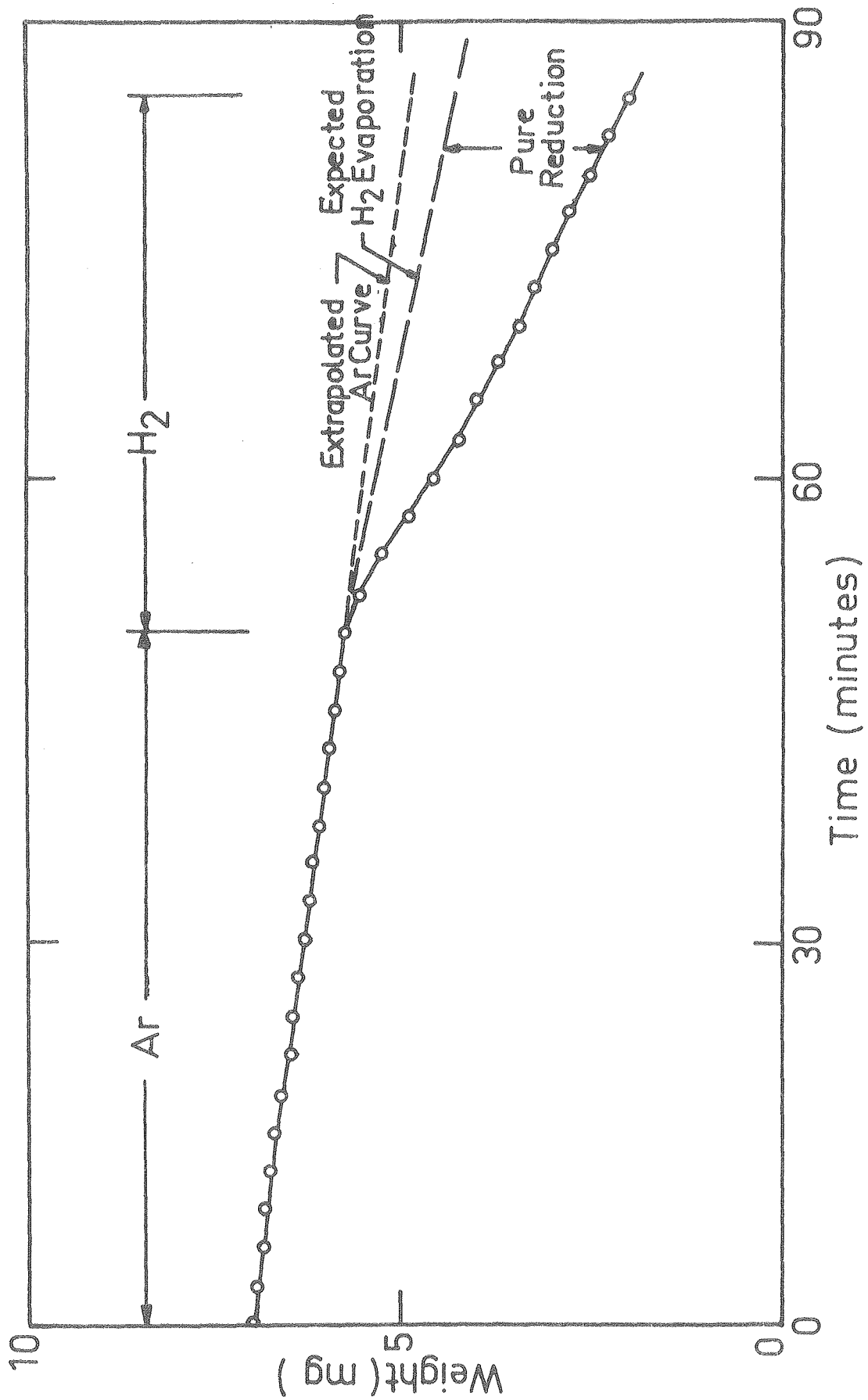
Weight (mg)
10
5
0
0
30
60
90
Time (minutes)
Ar
H2
Extrapolated Ar Curve
Expected H2 Evaporation
Pure Reduction

FIGURE 3

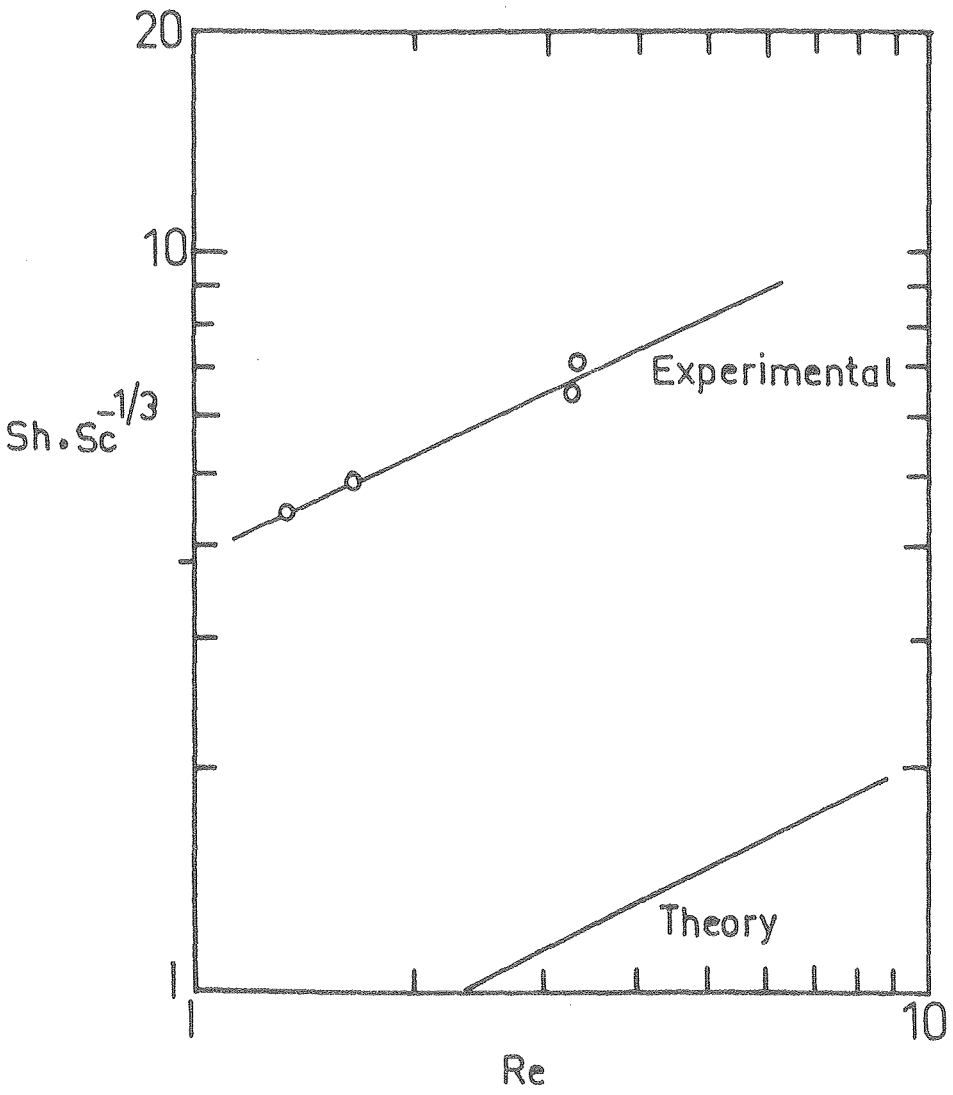

FIGURE 4

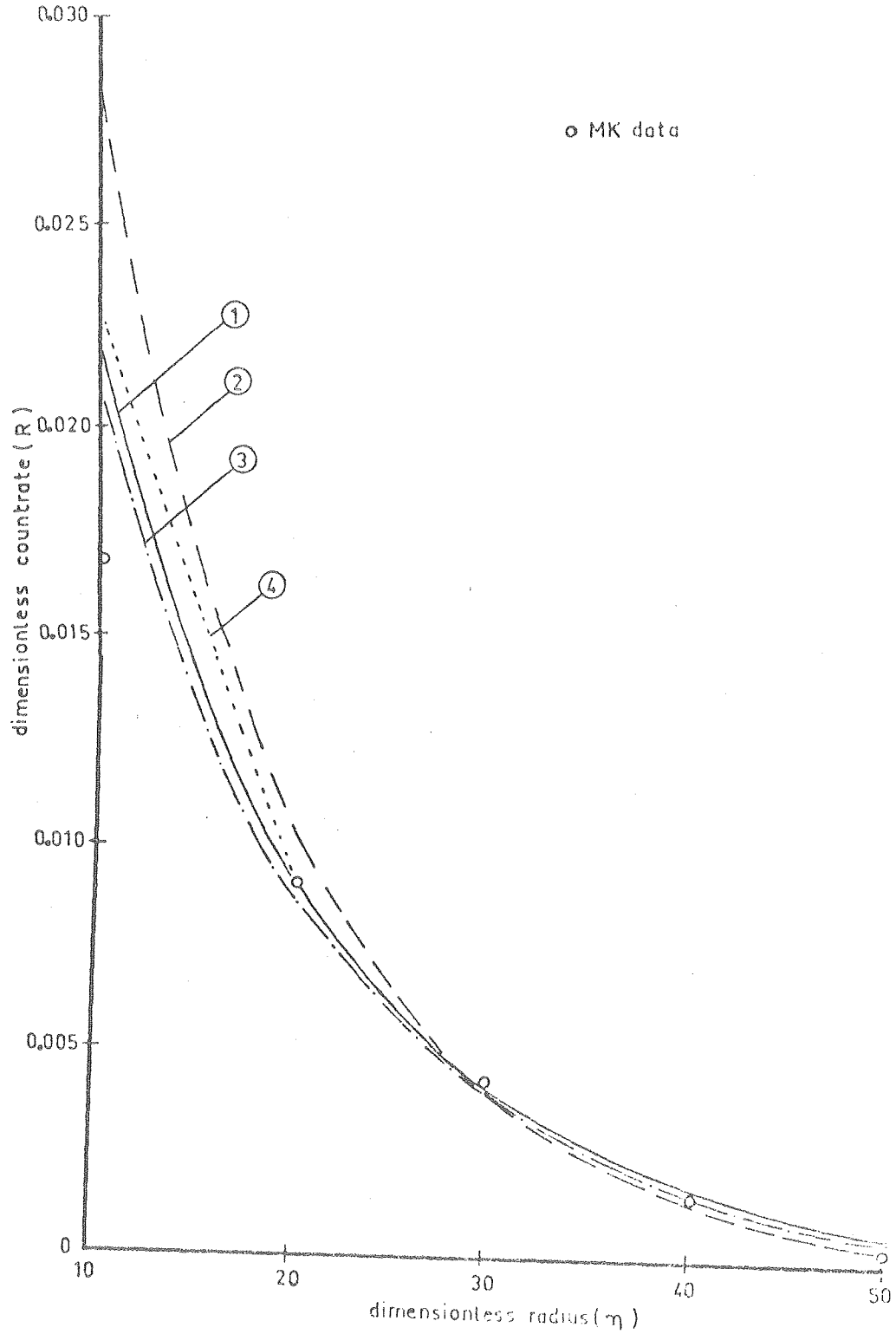
0.030
0.025
0.020
0.015
0.010
0.005
0
dimensionless countrate (R)
o MK data
1
2
3
4
10
20
30
40
50
dimensionless radius (η)

FIGURE 5

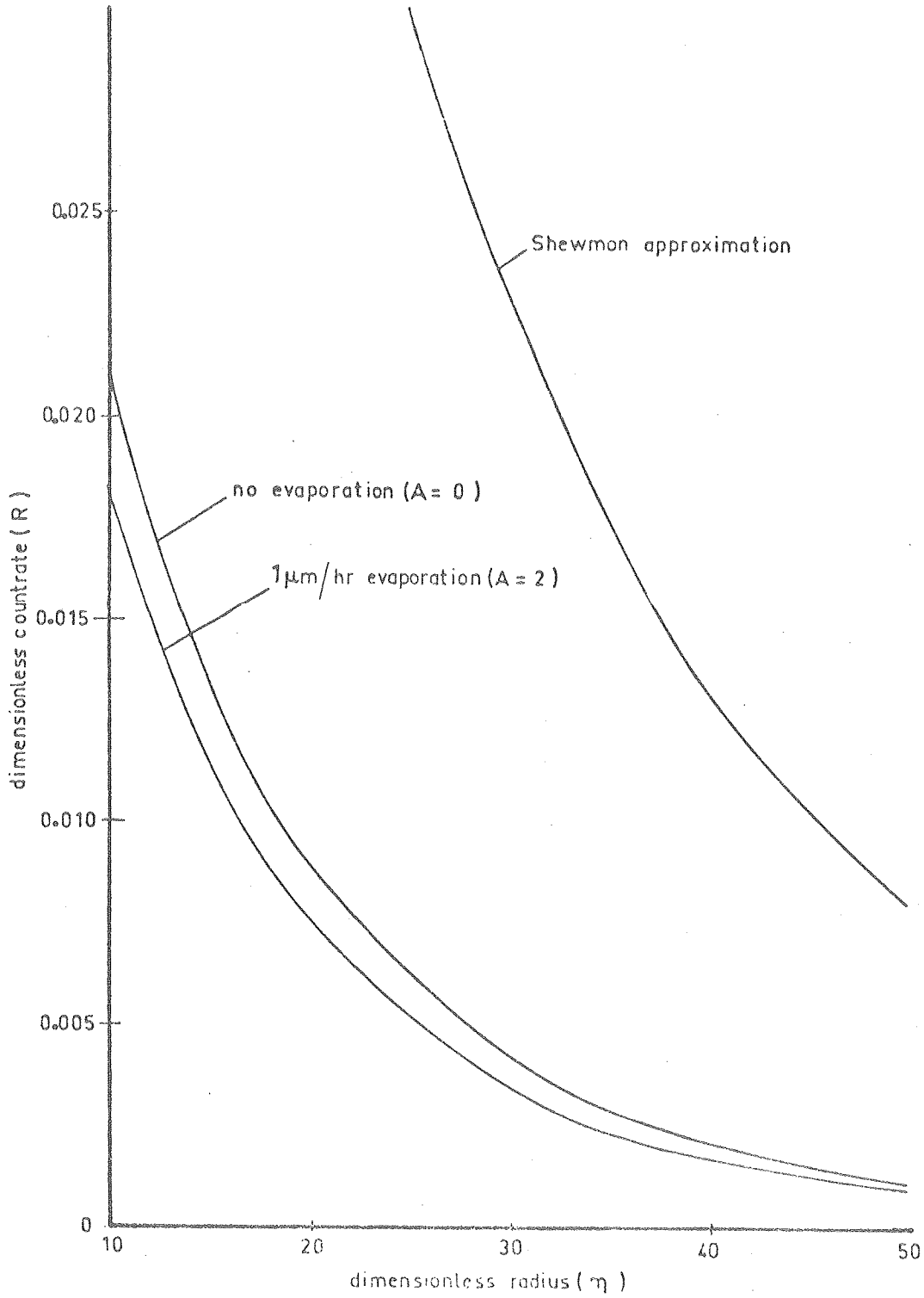
0.025
0.020
0.015
0.010
0.005
0
dimensionless countrate (R)
Shewmon approximation
no evaporation (A = 0)
1μm/hr evaporation (A = 2)
10
20
30
40
50
dimensionless radius (η)

FIGURE 6